Multimode quantum theory of nonlinear propagation in optical fibers

Aruto Hosaka, Taiki Kawamori, and Fumihiko Kannari
Department of Electronics and Electrical Engineering, Keio University, 3-14-1 Hiyoshi, Kohoku-ku, Yokohama 223-8522, Japan
(Received 13 June 2016; revised manuscript received 31 August 2016; published 17 November 2016)

We theoretically reveal the potential of the parallelism of squeezed state generation by nonlinear pulse propagation in an optical fiber. Starting from a nonlinear Schrödinger equation coupling with phonon modes that cause Raman noise, we develop a multimode quantum theory of nonlinear propagation in an optical fiber. Based on our proposed method, we numerically simulate fiber nonlinear propagation in two conditions: solitonlike and zero-group-delay-dispersion (zero-GVD) propagation. As a result, we find that zero-GVD propagation enables the large-scale parallel generation of squeezed states relative to solitonlike propagation owing to the broadband phase matching of the four-wave mixing process.

DOI: 10.1103/PhysRevA.94.053833

I. INTRODUCTION

In optical quantum information processing based on continuous variables such as amplitude and phase, a squeezed state is an essential element to generate entanglement states or cluster states [1,2]. Recently, to realize measurement-based quantum computing [3], based on various approaches, compact schemes for large-scale multimode squeezed or cluster state generation have been devised and experimentally demonstrated [4–11].

In all previous experiments, multimode squeezed state generation was achieved by a single or a pair of optical parametric oscillators (OPOs) utilizing the degrees of freedom of the photon field: frequency, wave vector, and polarization. The time and the wave front are the basis transformation of the frequency and the wave vector, respectively. The key to constructing a compact optical large-scale quantum network for practical quantum computers is how to utilize the degrees of freedom.

In this article, we study the multimode quantum theory of nonlinear fiber propagation. In previous research of single-mode squeezed state generation with a fiber, the highest squeezing level of −6.8 dB was demonstrated by nonlinear propagation in the anomalous dispersion regime of an optical fiber [12]. In the scheme of fiber-based squeezed state generation, a mode-locked laser pulse is employed as a pump source to induce a sufficient third-order nonlinear effect [12–17]. After propagation through a fiber, large-scale quantum correlations are formed among the frequency modes of the pulse through a four-wave mixing (FWM) process in the fiber [18,19]. Furthermore, the optical modes couple with phonon modes that cause thermal noise by Raman scattering [12,20,21]. Thus, to analyze multimode quantum propagation through the fiber, the evolution of the photon and phonon fields must be calculated [20–22].

In fact, the parallel generation of squeezed light with the Kerr effect was recently studied by Guo *et al.* [23]. However, phase matching approximation and assumption of an unchanged waveform of a propagating squeezed pulse were employed in this study. Furthermore, the Raman effect was not incorporated into this theory.

Therefore, we developed a multimode quantum theory to reveal the potential of parallel generation of squeezed states with a fiber nonlinear propagation that includes the Raman noise effect. Starting from a nonlinear Schrödinger equation (NSE) that includes Raman scattering, we propose a method that obtains a covariance matrix that represents the quantum correlation among frequency modes after nonlinear propagation through a fiber. Using Williamson's theorem and Euler decomposition, we analyzed the covariance matrix to obtain the separable modes of squeezed states [24]. Based on the developed theory, we demonstrated fiber-based multimode squeezed state generation by two numerical calculations: solitonlike and high-nonlinear zero-group-delay-dispersion (zero-GVD) propagation. By these numerical calculations, we discuss the potential of fiber-based multimode squeezed state generation for frequency-division multiplexed one-way quantum computing.

II. THEORY

Classical nonlinear propagation in an optical fiber can be described by NSE [22]:

$$\frac{\partial}{\partial z}A(z,t) = i\sum_{k\geqslant 2}\frac{i^k\beta_k}{k!}\frac{\partial^k}{\partial t^k}A(z,t) + i\gamma(1-f_r)|A(z,t)|^2A(z,t) + \frac{i\gamma f_r}{2g_0}\frac{\left(\Omega_0^2+\gamma_r^2\right)}{\Omega_0}[b(z,t)+b^*(z,t)]A(z,t). \quad (1)$$

Here, $A(z,t)$ is the classical complex amplitude in a fiber; t and z represent the time and position in a fiber; $b(z,t)$ is the amplitude of the phonon fields whose time evolution is given by $b(z,t) = ig_0\int_{-\infty}^{t}\exp[-(\gamma_r+i\Omega_0)(t-\tau)]|A(z,\tau)|^2d\tau$, where γ_r, Ω_0, and g_0 are the damping coefficient, the resonant frequency of a fiber, and the coupling coefficient of between the photon and phonon fields, respectively; γ and β_k in Eq. (1) are the nonlinear coefficient and the kth dispersion of a fiber, respectively; and f_r is the ratio of the contribution of Raman scattering.

Following [22], we quantize the photon and phonon fields. By the quantization of $A \to \hat{A}$ and $b \to \hat{b}$, the quantized time evolution of the phonon fields can be obtained:

$$\frac{\partial}{\partial z}b(z,t) = -\gamma_r\hat{b} - i\Omega_0\hat{b} + ig_0\hat{A}(z,t)\hat{A}^\dagger(z,t) + \hat{n}_b(z,t), \quad (2)$$

where $\hat{n}_b$ is the annihilation operator for the thermal reservoir and Eq. (2) represents coupling with a thermal reservoir by

damping of the phonon. This noise operator satisfies the bosonic commutation relation,

$$[\hat{n}_b(z,t),\hat{n}_b^\dagger(z',t')] = v\delta(z-z')\delta(t-t'), \tag{3}$$

and the four correlations

$$\begin{aligned}
&\langle\hat{n}_b(z,t)\hat{n}_b(z',t')\rangle = \langle\hat{n}_b^\dagger(z,t)\hat{n}_b^\dagger(z',t')\rangle = 0,\\
&\langle\hat{n}_b(z,t)\hat{n}_b^\dagger(z',t')\rangle = [n_\Omega(T)+1]v\delta(z-z')\delta(t-t'),\\
&\langle\hat{n}_b^\dagger(z,t)\hat{n}_b(z',t')\rangle = n_\Omega(T)v\delta(z-z')\delta(t-t'),
\end{aligned} \tag{4}$$

where $v = 4g_0^2\gamma_r\Omega_0/[f_r\gamma(\Omega_0^2+\gamma_r^2)]$. $n_\Omega(T)$ is the average phonon number in temperature T and $n_\Omega(T) = 1/[\exp(\hbar\Omega_0/k_BT)-1]$; $\hbar$ and k_B are the Dirac and Boltzmann constants, respectively.

By the decomposition of $\hat{A}$ into a mean value and perturbation $\hat{A} = A+\hat{a}$, a quantum linearized NSE can be obtained [20]:

$$\begin{aligned}
\frac{\partial}{\partial z}\hat{a}(z,t) = {}& i\sum_{k\geqslant 2}\frac{i^k\beta_k}{k!}\frac{\partial^k}{\partial t^k}\hat{a}(z,t) + 2i\gamma(1-f_r)|A(z,t)|^2\hat{a}(z,t)\\
&+ i\gamma(1-f_r)A^2(z,t)\hat{a}^\dagger(z,t)\\
&+ i\gamma f_r\int_{-\infty}^{t}h(t-\tau)|A(z,\tau)|^2d\tau\hat{a}(z,t)\\
&+ i\gamma f_r\int_{-\infty}^{t}h(t-\tau)A^*(z,\tau)\hat{a}(z,\tau)d\tau A(z,t)\\
&+ i\gamma f_r\int_{-\infty}^{t}h(t-\tau)A(z,\tau)\hat{a}^\dagger(z,\tau)d\tau A(z,t)\\
&+ i\frac{f_r\gamma}{2g_0}\int_{-\infty}^{t}[H(t-\tau)\hat{n}_b(z,\tau)\\
&+ H^*(t-\tau)\hat{n}_b^\dagger(z,\tau)]d\tau A(z,t),
\end{aligned} \tag{5}$$

where $H(t) = (\Omega_0^2+\gamma_r^2)/\Omega_0\times\exp[(-\gamma_r - i\Omega_0)t]$ and $h(t) = -\mathrm{Im}[H(t)]$. Thus output photon fields $\hat{a}(L,\omega)$ can be expressed by the linear combination of the input states in photon fields $\hat{a}(0,\omega)$ and the noise operators in phonon fields $\hat{n}_b(z,t)$:

$$\begin{aligned}
\hat{a}(L,\omega) = {}& \int_{-\infty}^{\infty}f(\omega,\omega')\hat{a}(0,\omega')d\omega'\\
&+ \int_{-\infty}^{\infty}g^*(\omega,\omega')\hat{a}^\dagger(0,\omega')d\omega'\\
&+ \int_0^L\int_{-\infty}^{\infty}f_R(\omega,z',t')\hat{n}_b(z',t')dt'dz'\\
&+ \int_0^L\int_{-\infty}^{\infty}g_R^*(\omega,z',t')\hat{n}_b^\dagger(z',t')dt'dz',
\end{aligned} \tag{6}$$

where L is the length of the fiber. Here, position z and frequency ω are respectively discretized into N and M slices [24]. After the discretization, $\hat{a}(z,\omega)$ can be expressed as $\hat{a}_m(n)$, where m and n represent the mth frequency division and nth position division.

Next, a vector of the creation-annihilation operators of the discretized photon and phonon fields are defined: $\hat{\mathbf{a}}(n) := [\hat{a}_1(n),\ldots,\hat{a}_M(n)]^\mathrm{T}$, $\hat{\mathbf{a}}^\dagger(n) := [\hat{a}_1^\dagger(n),\ldots,\hat{a}_M^\dagger(n)]^\mathrm{T}$, $\hat{\mathbf{n}}_b(n) := [\hat{n}_{b,1}(0),\ldots,\hat{n}_{b,m}(n'),\ldots,\hat{n}_{b,M}(n)]^\mathrm{T}$, and $\hat{\mathbf{n}}_b^\dagger(n) := [\hat{n}_{b,1}^\dagger(0),\ldots,\hat{n}_{b,m}^\dagger(n'),\ldots,\hat{n}_{b,M}^\dagger(n)]^\mathrm{T}$, respectively. Using these definitions, Eq. (5) can be rewritten:

$$\hat{\mathbf{a}}(N) = F\hat{\mathbf{a}}(0) + \bar{G}\hat{\mathbf{a}}^\dagger(0) + F_b\hat{\mathbf{n}}_b(0) + \bar{G}_b\hat{\mathbf{n}}_b^\dagger(0), \tag{7}$$

where F and G are $M\times M$ matrices and F_b and G_b are $M\times MN$ matrices. If the Raman scattering is ignored ($f_r = 0$), Eq. (7) can be reduced to $\hat{\mathbf{a}}(N) = F\hat{\mathbf{a}}(0) + \bar{G}\hat{\mathbf{a}}^\dagger(0)$, and these matrices can be decomposed into separable squeezed states of output modes and corresponding input coherent vacuums by Bloch-Messiah decomposition [25,26] (see Appendix A for details about calculation without Raman noise).

However, when Raman scattering is included in the calculation, we must obtain the covariance matrix and decompose it by Williamson's decomposition. To transform Eq. (7) into a description in phase space, first, we define the vectors of the amplitude and the phase quadrature of the photon and phonon fields, $\hat{\mathbf{x}}(n) := [\hat{\mathbf{a}}(n)+\hat{\mathbf{a}}^\dagger(n)]/\sqrt{2}$, $\hat{\mathbf{p}}(n) := [\hat{\mathbf{a}}(n)-\hat{\mathbf{a}}^\dagger(n)]/\sqrt{2}i$, $\hat{\mathbf{x}}_b(n) := [\hat{\mathbf{a}}_b(n)+\hat{\mathbf{a}}_b^\dagger(n)]/\sqrt{2}$, and $\hat{\mathbf{p}}_b(n) := [\hat{\mathbf{a}}_b(n)-\hat{\mathbf{a}}_b^\dagger(n)]/\sqrt{2}i$, respectively. We also define the $2M$ vector $\hat{\mathbf{r}} := [\hat{\mathbf{x}}^\mathrm{T}(n),\hat{\mathbf{p}}^\mathrm{T}(n)]^\mathrm{T}$ and the $2MN$ vector $\hat{\mathbf{r}}_b := [\hat{\mathbf{x}}_b^\mathrm{T}(n),\hat{\mathbf{p}}_b^\mathrm{T}(n)]^\mathrm{T}$. Using the quadrature operators, Eq. (7) can be rewritten:

$$\hat{\mathbf{r}}(N) = Z\hat{\mathbf{r}}(0) + Z_b\hat{\mathbf{r}}_b(0), \tag{8}$$

where

$$Z := \begin{pmatrix}\mathrm{Re}(F+G) & -\mathrm{Im}(F+G)\\ \mathrm{Im}(F-G) & \mathrm{Re}(F-G)\end{pmatrix}$$

and

$$Z_b := \begin{pmatrix}\mathrm{Re}(F_b+G_b) & -\mathrm{Im}(F_b+G_b)\\ \mathrm{Im}(F_b-G_b) & \mathrm{Re}(F_b-G_b)\end{pmatrix}.$$

The covariance matrix $C(n)$ is defined by anticommutation of the quadrature:

$$C(n) = \{\hat{\mathbf{r}}(n),\hat{\mathbf{r}}^\mathrm{T}(n)\}, \tag{9}$$

and if the input photon fields are coherent vacuums, from Eqs. (3), (4), (8), and (9), we obtain

$$C(N) = ZZ^\mathrm{T} + [2n_\Omega(T)+1]vZ_bZ_b^\mathrm{T}. \tag{10}$$

By Williamson's theorem, the covariance matrix $C(N)$ can be diagonalized [25]:

$$C(N) = S^\mathrm{T}\sigma S, \tag{11}$$

where $S\in\mathrm{Sp}(2M,\mathbb{R})$ and $\sigma = \oplus_{k=1}^M v_kE$. The diagonal matrix σ is called the *symplectic spectrum*, whose elements represent the purities of each separable mode. E represents the 2×2 identity matrix. The symplectic matrix S can also be diagonalized by Euler decomposition:

$$S = O_1\Lambda O_2, \tag{12}$$

where $O_1, O_2\in K(M) = \mathrm{Sp}(2M,\mathbb{R})\cap\mathrm{SO}(2M)$. The diagonal matrix $\Lambda = \oplus_{k=1}^M\left(\begin{smallmatrix}\lambda_k & 0\\ 0 & 1/\lambda_k\end{smallmatrix}\right)$ and denotes the local squeezers. O_2 corresponds to the separable output modes. Thus, the squeezing levels of each separable mode can be obtained from the covariance matrix $C'(N) = O_2^\mathrm{T}C(N)O_2$. Here, $C'(N)$ is not always a diagonal matrix, but the off-diagonal elements among individual modes represent not quantum inseparability but classical correlations.

III. CALCULATION RESULTS AND DISCUSSION

First, we calculated the solitonlike propagation in the anomalous dispersion regime of a conventional glass fiber used in the present optical communication networks. Since the propagating pulse can maintain its high peak power owing to the balance of the chromatic dispersion and the nonlinear effect in this regime, relatively high squeezing levels can be obtained [12]. In this calculation, we assumed a 39-cm single-mode silica fiber whose second-order dispersion β_2 and nonlinear coefficient γ were -20 ps^2/km and 2.0 W^{-1} km^{-1}. These parameters correspond those of a conventional single-mode glass fiber. The incident pulse was 125 fs (full width at half maximum) sech-shaped with a peak power of 2000 W. This pulse satisfies the soliton condition if the Raman parameter is ignored ($f_r = 0$), and the fiber length of 39 cm corresponds to one soliton period. We employed Raman scattering parameters that had been experimentally fitted [27]: $f_r = 0.18$, $1/\Omega_0 = 12.2$ (fs), and $1/\gamma_r = 32$ (fs). Moreover, we assumed the temperature of the fiber, T, was 300 K. We solved the NSE by the split-step Fourier method and numerically obtained the covariance matrix.

Figure 1(a) shows the normalized covariance matrix $C_{ij}^{(n)} = C_{ij}/\sqrt{C_{ii}C_{jj}} - \delta_{ij}/C_{ij}$. Referring to previous work [28], we calculated the symplectic matrix S that diagonalizes the covariance matrix. Then we obtained the complex spectrum and the squeezing levels of each separable squeezed pulse by Euler decomposition [Figs. 1(b) and 1(c)]. The spectral phases in Fig. 1(c) correspond to the squeezing angle. Figure 1(d) shows the spectral phase and the amplitude of the classical input and output pulses.

From these results, we found that the separable squeezed pulse became a negatively chirped Hermite-Gaussian-like

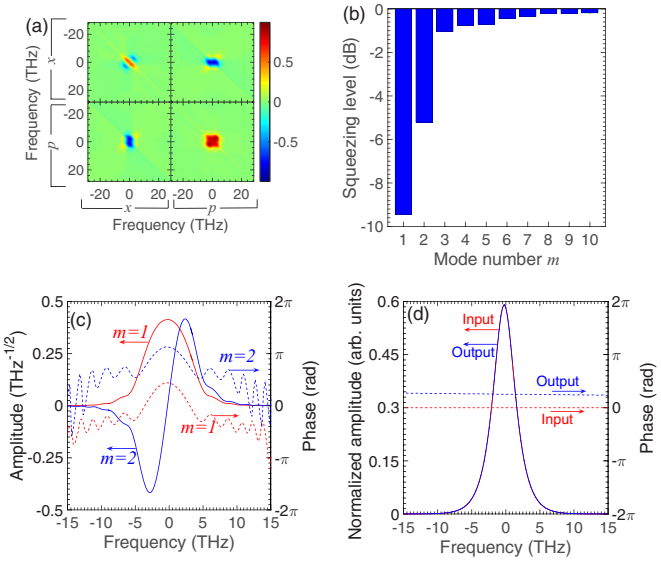

FIG. 1. Calculation results when we assumed solitonlike propagation through the 39-cm fiber: (a) normalized covariance matrix $C^{(n)}$; (b) squeezing levels of each separable squeezed state. These modes were arranged in ascending order: (c) spectra of first and second squeezed modes and (d) normalized spectra of classical input and output pulses.

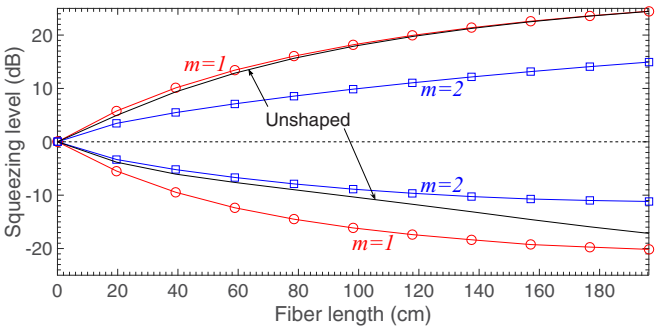

FIG. 2. Squeezing levels of first (red circles) and second (blue squares) squeezed modes versus length of silica fiber. Black lines show squeezing and antisqueezing levels when unshaped classical output pulse was employed as a local oscillator.

spectrum. Furthermore, only two modes were squeezed. This is because the broadband phase matching condition is not satisfied due to chromatic dispersion.

In Fig. 2, the red circles and blue squares respectively indicate the squeezing and antisqueezing levels of the first and second modes versus fiber length L. Black solid lines show the squeezing and antisqueezing levels when unshaped classical output pulses were employed as a local oscillator (LO), like in conventional schemes [11–16]. These noise levels in the conventional schemes were calculated from a normalized classical output spectrum and covariance matrix C (see details in Appendix B). As shown in Fig. 2, the squeezing levels saturate at about -20 dB. Since no such saturation was observed in the calculation of 196-cm propagation without Raman scattering, this is clearly an effect of Raman scattering. Here, because the peak power after propagation of the 196-cm fiber was 2020 W, this is not due to a decrease of peak power caused by chromatic dispersion. Accordingly, we infer that this is due to the balance between squeezing by the nonlinear effect and additional noise by Raman scattering.

Next, assuming high-nonlinear zero-GVD photonic crystal fiber (PCF) that is well employed in an experiment of supercontinuum generation, we performed a similar calculation as those done for soliton propagation. In a previous experiment of squeezed light generation with a PCF, -3.9 dB polarization squeezing [29] and -4.6 dB photon-number squeezing [30] were reported, but these squeezing levels are low relative to experiments of solitonlike pulses. However, the broadband phase matching condition of FWM can be satisfied in nonlinear propagation in a PCF due to small chromatic dispersion. In our calculation, we assumed a PCF employed in our previous experiment [30]. The fiber parameters were $\beta_2 = 0$ ps^2/km, $\beta_3 = 0.162$ ps^3/km, $\beta_4 = 1.934 \times 10^{-4}$ ps^4/km, and $\gamma = 46.8$ W^{-1} km^{-1}. The parameters of a pump pulse and Raman scattering were identical to the calculation of the solitonlike propagation in the anomalous dispersion regime. Figure 3 shows the calculation results when fiber length L is 15 mm. As shown in this figure, the first frequency mode exhibits -10 dB squeezing after 15 mm propagation in the PCF. This squeezing level is almost the same as that obtained at one-soliton length propagation in the conventional single-mode fiber, which was shown in Fig. 1(b). Therefore, we may provide proper comparison in squeezed mode generation between

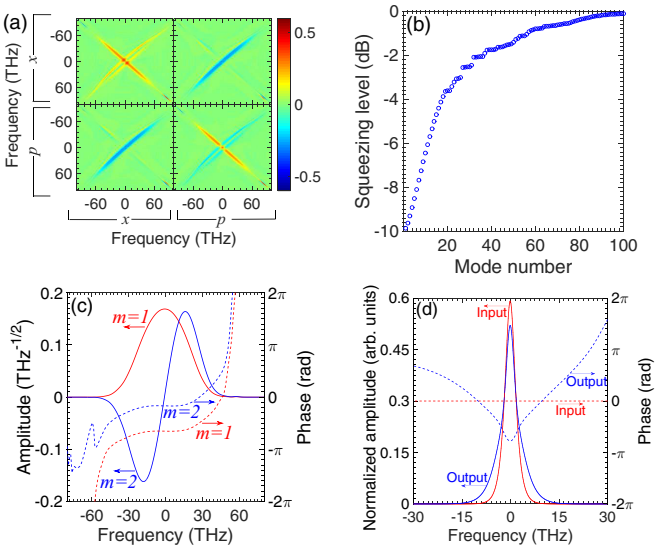

FIG. 3. Calculation results when we assumed zero-GVD propagation through 15-mm PCF: (a) normalized covariance matrix $C^{(n)}$ and (b) squeezing levels of each separable squeezed state. These modes are arranged in ascending order: (c) spectra of first and second squeezed modes and (d) normalized spectra of classical input and output pulses.

soliton and zero-GVD propagation with these parameters for numerical calculations with the PCF fiber. In Fig. 3(b), the number of squeezed modes became larger relative to solitonlike propagation because a broader quantum correlation was formed. Furthermore, similar to the case of solitonlike propagation, the spectral amplitude of the squeezed pulses became Hermite-Gaussian shaped, and the spectral phase reflected the PCF's chromatic dispersion [Fig. 3(c)]. Note that the spectra of the eigenmodes were much broader than those of the classical output pulse [Fig. 3(d)]. In Fig. 3(c), due to this significant spectral mismatching between the squeezed modes and the classical output pulses, the squeezing levels substantially deteriorated in the conventional schemes in which a classical output pulse was employed as a LO.

Figure 4 shows the calculation results of the propagation length versus the squeezing levels of the first (red circles), sixth (blue squares), 11th (green diamonds), and 16th modes (cyan triangles). Black solid lines show squeezing and antisqueezing levels when an unshaped classical output pulse was employed as a LO. The squeezing levels of the high-order modes became high relative to the soliton propagation. However, the squeezing levels of the high-order modes are saturated due to the proportionality relation between the chromatic dispersion and the fiber length. Shorter fiber and a higher-peak pulse must be chosen to obtain higher squeezing levels of the high-order modes.

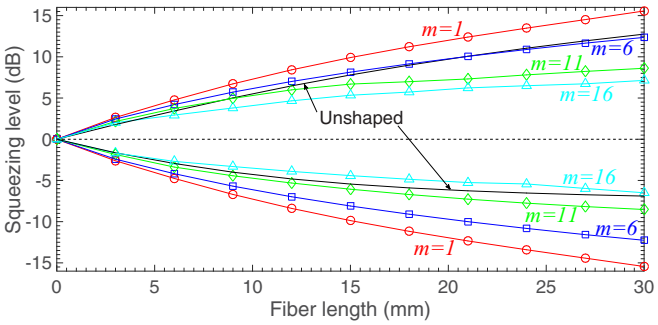

FIG. 4. Squeezing levels of first (red circles), sixth (blue squares), 11th (green diamonds), and 16th (cyan triangles) squeezed modes versus length of silica fiber. Black lines show squeezing and antisqueezing levels when an unshaped classical output pulse was employed as a LO.

IV. CONCLUSION

We numerically demonstrated multimode squeezed state generation by fiber nonlinear propagation based on a theory we developed. Our results imply that a large-scale wavelength-division-multiplexed quantum network for a one-way quantum computer can be realized with a simple fiber-based scheme.

We found that two separable squeezed states were generated by solitonlike propagation conventionally used in previous researches. By our numerical analysis, we observed the limits of squeezing level due to Raman noise.

Furthermore, we revealed that the large-scale parallel generation of squeezed states was possible by zero-dispersion nonlinear propagation owing to broadband phase matching of FWM. No high squeezing level was obtained in previous experiments with PCF relative to solitonlike propagation. However, this result was due to significant mismatching of the spectra between the LO and squeezed pulses.

Squeezed pulse modes generated in parallel in the frequency domain are overlapped in both the time and the spatial domains. Since Gaussian quantum computing can be achieved by postselection using homodyne measurements [31], even if those frequency modes remain spatiotemporally overlapping, they are still useful. However, in universal one-way quantum computing, mode extraction by quantum pulse gating [32,33] may be necessary to spatially separate arbitrary modes for non-Gaussian measurement (e.g., photon counting).

In our calculation, we assumed a sech-shaped specific pump pulse and discussed the quantum correlation that was formed among the output frequency modes. However, a better pump pulse may exist that enhances the squeezing levels and the number of squeezed modes. Such a pump pulse will be found by adaptive shaping of its spectrum [34].

ACKNOWLEDGMENTS

We thank Masahiro Takeoka for his helpful discussion. This research was supported by JSPS KAKENHI Grant No. 15K13385 and Grant-in-Aid for JSPS Fellows No. 16J03900.

APPENDIX A: NONLINEAR PROPAGATION WITHOUT RAMAN SCATTERING

In this section, we discuss nonlinear propagation without Raman scattering ($f_r = 0$). If $f_r = 0$, the quantum NSE can be reduced:

$$\frac{\partial}{\partial z}\hat{a}(z,t) = i\sum_{k\geqslant 2}\frac{i^k\beta_k}{k!}\frac{\partial^k}{\partial t^k}\hat{a}(z,t) + 2i\gamma|A(z,t)|^2\hat{a}(z,t) + i\gamma A^2(z,t)\hat{a}^\dagger(z,t). \quad \text{(A1)}$$

Similar to the calculation with Raman scattering, the output quantum state after propagation through an optical fiber can be represented by the sum of the input coherent vacuum:

$$\hat{a}(L,\omega) = \int_{-\infty}^{\infty} f(\omega,\omega')\hat{a}(0,\omega')d\omega' + \int_{-\infty}^{\infty} g^*(\omega,\omega')\hat{a}^\dagger(0,\omega')d\omega'. \quad \text{(A2)}$$

By discretization of the frequency modes and the position in the fiber, Eq. (A1) can be rewritten into matrix notation:

$$\hat{\mathbf{a}}(N) = F\hat{\mathbf{a}}(0) + \bar{G}\hat{\mathbf{a}}^\dagger(0). \quad \text{(A3)}$$

By Bloch-Messiah decomposition, we can decompose F and G^* into two unitary rotation matrices, U, V, and diagonal real matrices $A_D = \mathrm{diag}\{a_1,\ldots,a_N\}$, $B_D = \mathrm{diag}\{b_1,\ldots,b_N\}$ [26]:

$$F = UA_DV^*, \quad \bar{G} = UB_DV^{\mathrm{T}}, \quad \text{(A4)}$$

where a pair of diagonal matrices satisfies $A_D^2 = B_D^2 + E$, where E is the $N \times N$ identity matrix. Unitary rotation matrices U and V represent the basis of the input coherent vacuum and the corresponding separable squeezed states. Bloch-Messiah decomposition is equivalent to Euler decomposition. If Raman scattering is not included in the NSE, we can obtain the following equation:

$$\hat{\mathbf{r}}(N) = Z\hat{\mathbf{r}}(0). \quad \text{(A5)}$$

Since Z is a symplectic matrix, we can diagonalize it by Euler decomposition:

$$Z = O'\Lambda O'', \quad \text{(A6)}$$

where $O_1, O_2 \in K(M) = \mathrm{Sp}(2M,\mathbb{R}) \cap \mathrm{SO}(2M)$. Λ is a diagonal matrix: $\Lambda = \otimes_{k=1}^{M} \begin{pmatrix} 1/\lambda_k & 0 \\ 0 & \lambda_k \end{pmatrix}$. If Eq. (A6) is substituted into Eq. (A5), we can obtain a new basis of input and output modes:

$$O'^{\mathrm{T}}\hat{\mathbf{r}}(N) = \Lambda O''\hat{\mathbf{r}}. \quad \text{(A7)}$$

Here, we define the vectors of amplitude and phase quadrature:

$$O'^{\mathrm{T}}\hat{\mathbf{r}}(N) := \hat{\mathbf{u}}, \quad O''\hat{\mathbf{r}}(0) := \hat{\mathbf{v}}, \quad \text{(A8)}$$

where $\hat{\mathbf{u}} = (\hat{u}_{x,1},\hat{u}_{p,1},\ldots,\hat{u}_{x,M},\hat{u}_{p,M})^{\mathrm{T}}$ and $\hat{\mathbf{v}} = (\hat{v}_{x,1},\hat{v}_{p,1},\ldots,\hat{v}_{x,M},\hat{v}_{p,M})^{\mathrm{T}}$. As a result, the following simple relation can be derived:

$$\hat{u}_{x,m} = \frac{1}{\lambda_m}\hat{v}_{x,m}, \quad \hat{u}_{p,m} = \lambda_m\hat{v}_{p,m}. \quad \text{(A9)}$$

Thus, unlike the case of the calculation with Raman noise, we can directly obtain the basis and corresponding squeezing levels of the independent input coherent vacuum and the output squeezed modes from Euler decomposition. First, we calculated the propagation of the soliton pulse of a 39-cm fiber. The parameters of the fiber and input pulse were identical to those employed in the calculation with Raman scattering. These parameters satisfy the conditions of soliton propagation. A fiber length of 39 cm corresponds to a one-soliton period. Figure 5 shows the calculation results, and Fig. 5(a) shows the normalized covariance matrix. Figure 5(b) shows the squeezing levels of each separable squeezed state given by $-20\log_{10}\lambda_m$. Figures 5(c) and 5(d) respectively show the complex spectra of input coherent vacuum $\hat{v}_{x,m}$ (blue lines) and separable squeezed modes $\hat{u}_{x,m}$ (red lines) when $m = 1$ and

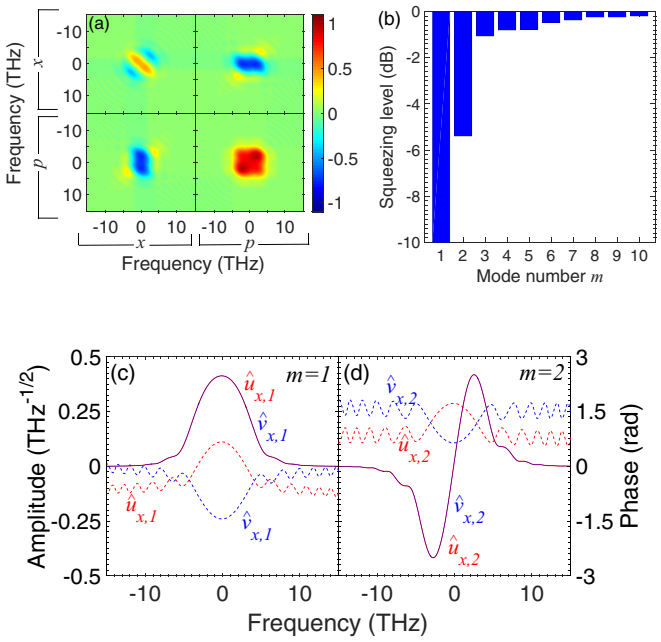

FIG. 5. Calculation results of 39-cm soliton propagation: (a) normalized covariance matrix $C^{(n)}$; (b) squeezing levels of each separable squeezed state given by $-20\log_{10}\lambda_m$; and complex spectra of input coherent vacuum $hat v_{x,m}$ (blue lines) and separable squeezed modes $\hat{u}_{x,m}$ (red lines) when (c) $m = 1$ and (d) $m = 2$, respectively.

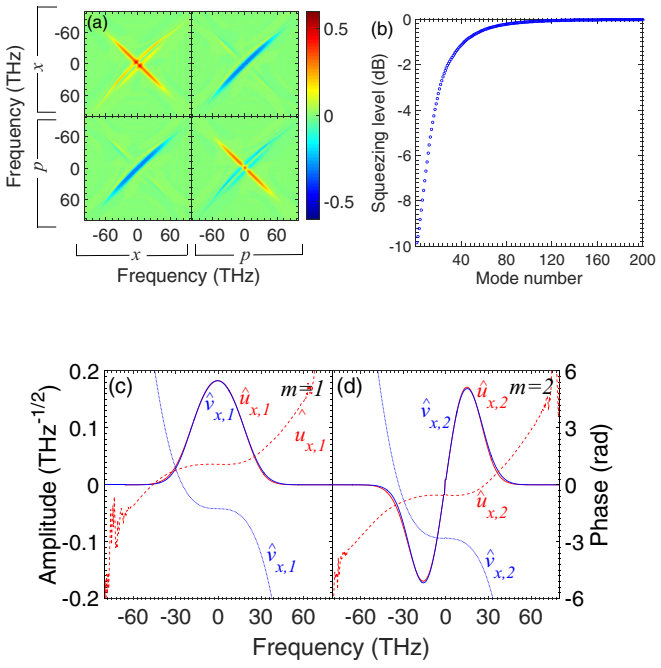

FIG. 6. Calculation results of nonlinear propagation in 15-mm zero-dispersion fiber: (a) normalized covariance matrix $C^{(n)}$; (b) squeezing levels of each separable squeezed state given by $-20\log_{10}\lambda_m$; and complex spectra of input coherent vacuum $\hat{v}_{x,m}$ (blue lines) and separable squeezed modes $\hat{u}_{x,m}$ (red lines) when (c) $m = 1$ and (d) $m = 2$, respectively.

$m = 2$. The spectral amplitudes of the input and output pulses were consistent, and their spectral phases were symmetric with respect to the phase axis.

Next, we calculated the propagation in the 15-mm zero-dispersion fiber. The parameters of the fiber and input pulse were identical to those in the calculation with Raman scattering. Figure 6 shows the calculation results, and Fig. 6(a) shows the normalized covariance matrix. Figure 6(b) shows the squeezing levels of each separable squeezed state given by $-20\log_{10}\lambda_m$. Figures 6(c) and 6(d) respectively show the complex spectra of input coherent vacuum $\hat{v}_{x,m}$ (blue lines) and separable squeezed modes $\hat{u}_{x,m}$ (red lines) when $m = 1$ and $m = 2$. Similar to the calculation of soliton propagation, the spectral amplitudes of the input and output modes almost overlapped. On the other hand, the spectral phases of the input and output modes were shaped like negative and positive third-order dispersions, but they were not symmetric with respect to the phase axis.

APPENDIX B: SQUEEZING LEVELS IN CONVENTIONAL SCHEMES

In this section, we discuss a method that calculates the squeezing and antisqueezing levels obtained in the conventional schemes in which the classical output pulse through the fiber is employed as a LO. First, we discretize the classical output pulse as $A(L,\omega) \to \mathbf{A}(N) = [A(N,1),\ldots,A(N,M)]^{\mathrm{T}}$. Now, we define the normalized classical output pulse:

$$\mathbf{A}^{(n)} = \frac{\mathbf{A}(N)}{||\mathbf{A}(N)||_2}, \tag{B1}$$

where $||\mathbf{A}(N)||_2$ is the L^2 norm of the vector of the output pulse. Next, we define two $2M$ vectors of the LOs as follows:

$$\mathbf{A}_x = (\mathrm{Re}[\mathbf{A}^{(n)}],\mathrm{Im}[\mathbf{A}^{(n)}]), \quad \mathbf{A}_p = (-\mathrm{Re}[\mathbf{A}^{(n)}],\mathrm{Im}[\mathbf{A}^{(n)}]). \tag{B2}$$

Next, we calculate the 2×2 covariance matrix $C = \begin{pmatrix} C_{xx} & C_{xp} \\ C_{xp} & C_{pp} \end{pmatrix}$, projected from the $2M \times 2M$ covariance matrix $C(N)$ by the LO. This projection can be calculated by

$$\begin{aligned} &C_{xx} = \mathbf{A}_x^{\mathrm{T}} C(N) \mathbf{A}_x, \quad C_{pp} = \mathbf{A}_p^{\mathrm{T}} C(N) \mathbf{A}_p, \\ &C_{xp} = [(\mathbf{A}_x + \mathbf{A}_p)^{\mathrm{T}} C(N)(\mathbf{A}_x + \mathbf{A}_p) - C_{xx} - C_{pp}]/2, \end{aligned} \tag{B3}$$

where C_{xx} corresponds to the photon-number noise of the output pulses. Since the fiber nonlinear effect and Raman scattering do not change the photon numbers of a propagating pulse, $C_{xx} = 1$. The eigenvalues of the 2×2 covariance matrix C correspond to the squeezing and antisqueezing noise variances.

[1] A. Heidmann, R. J. Horowicz, S. Reynaud, E. Giacobino, C. Fabre, and G. Camy, Phys. Rev. Lett. **59**, 2555 (1987).
[2] M. Yukawa, R. Ukai, P. van Loock, and A. Furusawa, Phys. Rev. A **78**, 012301 (2008).
[3] N. C. Menicucci, P. van Loock, M. Gu, C. Weedbrook, T. C. Ralph, and M. A. Nielsen, Phys. Rev. Lett. **97**, 110501 (2006).
[4] M. Pysher, Y. Miwa, R. Shahrokhshahi, R. Bloomer, and O. Pfister, Phys. Rev. Lett. **107**, 030505 (2011).
[5] M. Chen, N. C. Menicucci, and O. Pfister, Phys. Rev. Lett. **112**, 120505 (2014).
[6] S. Yokoyama, R. Ukai, S. C. Armstrong, C. Sornphiphatphong, T. Kaji, S. Suzuki, J. Yoshikawa, H. Yonezawa, N. C. Menicucci, and A. Furusawa, Nat. Photonics **7**, 982 (2013).
[7] M. Lassen, V. Delaubert, J. Janousek, K. Wagner, H. A. Bachor, P. K. Lam, N. Treps, P. Buchhave, C. Fabre, and C. C. Harb, Phys. Rev. Lett. **98**, 083602 (2007).
[8] S. Armstrong, J.-F. Morizur, J. Janousek, B. Hage, N. Treps, P. K. Lam, and H.-A. Bachor, Nat. Commun. **3**, 1026 (2012).
[9] O. Pinel, P. Jian, R. M. de Araujo, J. Feng, B. Chalopin, C. Fabre, and N. Treps, Phys. Rev. Lett. **108**, 083601 (2012).
[10] J. Roslund, M. De Arau, S. Jiang, C. Fabre, and N. Treps, Nat. Photonics **8**, 109 (2014).
[11] R. Medeiros de Araujo, J. Roslund, Y. Cai, G. Ferrini, C. Fabre, and N. Treps, Phys. Rev. A **89**, 053828 (2014).
[12] R. Dong, J. Heersink, J. F. Corney, P. D. Drummond, U. L. Andersen, and G. Leuchs, Opt. Lett. **33**, 116 (2008).
[13] K. Bergman and H. A. Haus, Opt. Lett. **16**, 663 (1991).
[14] C. X. Yu, H. A. Haus, and E. P. Ippen, Opt. Lett. **26**, 669 (2001).
[15] M. Rosenbluh and R. M. Shelby, Phys. Rev. Lett. **66**, 153 (1991).
[16] J. Heersink, T. Gaber, S. Lorenz, O. Glockl, N. Korolkova, and G. Leuchs, Phys. Rev. A **68**, 013815 (2003).
[17] J. Heersink, V. Josse, G. Leuchs, and U. L. Andersen, Opt. Lett. **30**, 1192 (2005).
[18] A. Hosaka, K. Hirosawa, R. Sawada, and F. Kannari, Opt. Express **23**, 18850 (2015).
[19] S. Spalter, N. Korolkova, F. Konig, A. Sizmann, and G. Leuchs, Phys. Rev. Lett. **81**, 786 (1998).
[20] P. D. Drummond and J. F. Corney, J. Opt. Soc. Am. B **18**, 139 (2001).
[21] J. F. Corney and P. D. Drummond, J. Opt. Soc. Am. B **18**, 153 (2001).
[22] Y. Lai and S. S. Yu, Phys. Rev. A **51**, 817 (1995).
[23] X. Guo, N. Liu, X. Li, and Z. Y. Ou, Opt. Express **23**, 29369 (2015).
[24] M. Fiorentino, J. E. Sharping, P. Kumar, C. Universitario, M. S. Angelo, and G. Edificio, Opt. Express **10**, 128 (2002).
[25] G. Adesso, Open Syst. Inf. Dyn. **21**, 1440001 (2014).
[26] S. L. Braunstein, Phys. Rev. A **71**, 055801 (2005).
[27] R. H. Stolen, J. P. Gordon, W. J. Tomlinson, and H. A. Haus, J. Opt. Soc. Am. B **6**, 1159 (1989).
[28] S. Pirandola, A. Serafini, and S. Lloyd, Phys. Rev. A **79**, 052327 (2009).
[29] J. Milanović, M. Lassen, U. L. Andersen, and G. Leuchs, Opt. Express **18**, 1521 (2010).
[30] K. Hirosawa, H. Furumochi, A. Tada, F. Kannari, M. Takeoka, and M. Sasaki, Phys. Rev. Lett. **94**, 203601 (2005).
[31] G. Ferrini, J. P. Gazeau, T. Coudreau, C. Fabre, and N. Treps, New J. Phys. **15**, 093015 (2013).
[32] B. Brecht, A. Eckstein, A. Christ, H. Suche, and C. Silberhorn, New J. Phys. **13**, 065029 (2011).
[33] B. Brecht, A. Eckstein, R. Ricken, V. Quiring, H. Suche, L. Sansoni, and C. Silberhorn, Phys. Rev. A **90**, 030302(R) (2014).
[34] D. Fujishima, F. Kannari, M. Takeoka, and M. Sasaki, Opt. Lett. **28**, 275 (2003).